Cell, Vol. 94, 439–449, August 21, 1998, Copyright ©1998 by Cell Press

Crystal Structure of a GCN5-Related N-acetyltransferase: *Serratia marcescens* Aminoglycoside 3-N-acetyltransferase

Eva Wolf,* Alex Vassilev,‡ Yasutaka Makino,‡‖ Andrej Sali,* Yoshihiro Nakatani,‡ and Stephen K. Burley*†§
*Laboratories of Molecular Biophysics
†Howard Hughes Medical Institute
The Rockefeller University
New York, New York 10021
‡Laboratory of Molecular Growth Regulation
National Institute of Child Health and Human Development
National Institutes of Health
Bethesda, Maryland 20892

Summary

The X-ray structure of a canonical GCN5-related N-acetyltransferase (GNAT), *Serratia marcescens* aminoglycoside 3-N-acetyltransferase, bound to coenzyme A (CoA) has been determined at 2.3 Å resolution. The single domain α/β protein resembles a cupped right hand wrapped around a cylinder and consists of a highly curved, six-stranded β sheet of mixed polarity that is sandwiched between four α helices. The structure includes all four conserved GNAT motifs (C, D, A, and B) and represents the catalytic core of this large enzyme superfamily. Acetyl CoA recognition is mediated by a βα structure derived from GNAT motif A, which presents an invariant Arg/Gln-X-X-Gly-X-Gly/Ala segment for hydrogen bonding with the cofactor. Motif B contributes acidic residues to the binding site for the positively charged antibiotic substrate.

Introduction

Since Allfrey et al. (1964) demonstrated that enzyme-catalyzed acetylation of the basic N-terminal tails of core histones could affect eukaryotic gene expression, considerable efforts have been made to identify and characterize the responsible acetyl coenzyme A–dependent N-acetyltransferases. Research in diverse areas, including bacterial antibiotic resistance, the neurobiology of human circadian rhythms, gene expression, and DNA replication and packaging, has uncovered an impressive example of divergent evolution. More than 150 distinct enzymes, derived from every kingdom of life, appear to have evolved from a common ancestral N-acetyltransferase (or NAT) and are referred to as the GCN5-related NATs or GNATs (Neuwald and Landsman, 1997).

Figure 1 illustrates sequence alignments of a representative subset of the GNATs with diverse substrate specificity. Four conserved sequence motifs (C, D, A, and B) are characteristic of the GNATs, with motif A varying the least among superfamily members. In the midst of motif A, lies an invariant Arg/Gln-X-X-Gly-X-Gly/Ala segment (X denotes some variation). Site-directed mutagenesis of one or more of these three conserved residues dramatically reduces in vitro NAT activity of human spermidine/spermine NAT (Coleman et al., 1996; Lu et al., 1996), yeast GCN5 (Kuo et al., 1998; Wang et al., 1998), and ESA1 (Smith et al., 1998). Additional studies in vivo with two genes encoding putative NATs (yeast *mak3* and *Drosophila mof*) demonstrated significant biological effects of analogous mutations (Tercero et al., 1992; Hilfiker et al., 1997). Quantitative characterization of the effects of simultaneous mutation of the two conserved glycine residues in human spermidine/spermine NAT documented reduced binding affinity for acetyl coenzyme A (AcCoA) (Lu et al., 1996), suggesting that the invariant segment plays a critical role in cofactor binding. In the absence of a three-dimensional structure of any member of the GNAT superfamily, Lu et al. (1996) examined sequence conservation in the flanking regions and predicted that this putative AcCoA-binding segment adopts a βα structure.

Within the GNAT superfamily there is a subgroup of eubacterial aminoglycoside N-acetyltransferases (AATs), which catalyze acetyl group addition to aminoglycoside antibiotics directed against aerobic, gram-negative bacilli (reviewed in Shaw et al., 1993). The AATs are of considerable interest in clinical medicine because of the growing problem of broad-spectrum aminoglycoside resistance, which tends to be correlated with aggregate levels of aminoglycoside usage (reviewed in Miller et al., 1997). Acquisition of any one of the AATs typically provides the bacterium with resistance against most of the commonly used aminoglycosides, including gentamicin, tobramycin, and netilmicin. Figure 1 illustrates sequence alignments of representative AATs, which catalyze acetyl group addition to one of three distinct amino groups (designated 3, 2′, and 6′) found in aminoglycoside antibiotics. The three archetypal AATs are similar in sequence within the four GNAT motifs, suggesting that a three-dimensional structure of any one of these enzymes will provide valuable information regarding the molecular bases of N-acetyltransferase–mediated aminoglycoside resistance.

Here, we present the 2.3 Å resolution X-ray structure of *Serratia marcescens* aminoglycoside-3-N-acetyltransferase (AAT) (Javier Teran et al., 1992) bound to CoA. Our work provides a structure for the canonical N-acetyltransferase fold common to all GCN5-related N-acetyltransferases. The α/β protein resembles a cupped right hand wrapped around a narrow cylinder and consists of a highly curved, six-stranded β sheet of mixed polarity sandwiched between three short α helices on one face and one long α helix on the other. The structure includes all four motifs (C, D, A, and B) conserved among the GNATs and represents the catalytic core of this large superfamily of biologically important enzymes. The protein's concave surface contains the AcCoA-binding notch, created by apposition of the long α helix and the β sheet. The Arg/Gln-X-X-Gly-X-Gly/Ala segment found in motif A supports recognition of the 3′-phosphate ADP portion of the cofactor, via an intricate network of hydrogen bonds donated by main chain amino groups and a

§To whom correspondence should be addressed.
‖Present address: Department of Biology, Faculty of Science, Chiba University, 1-33 Yayoi-cho, Inage-ku, Chiba, Japan.

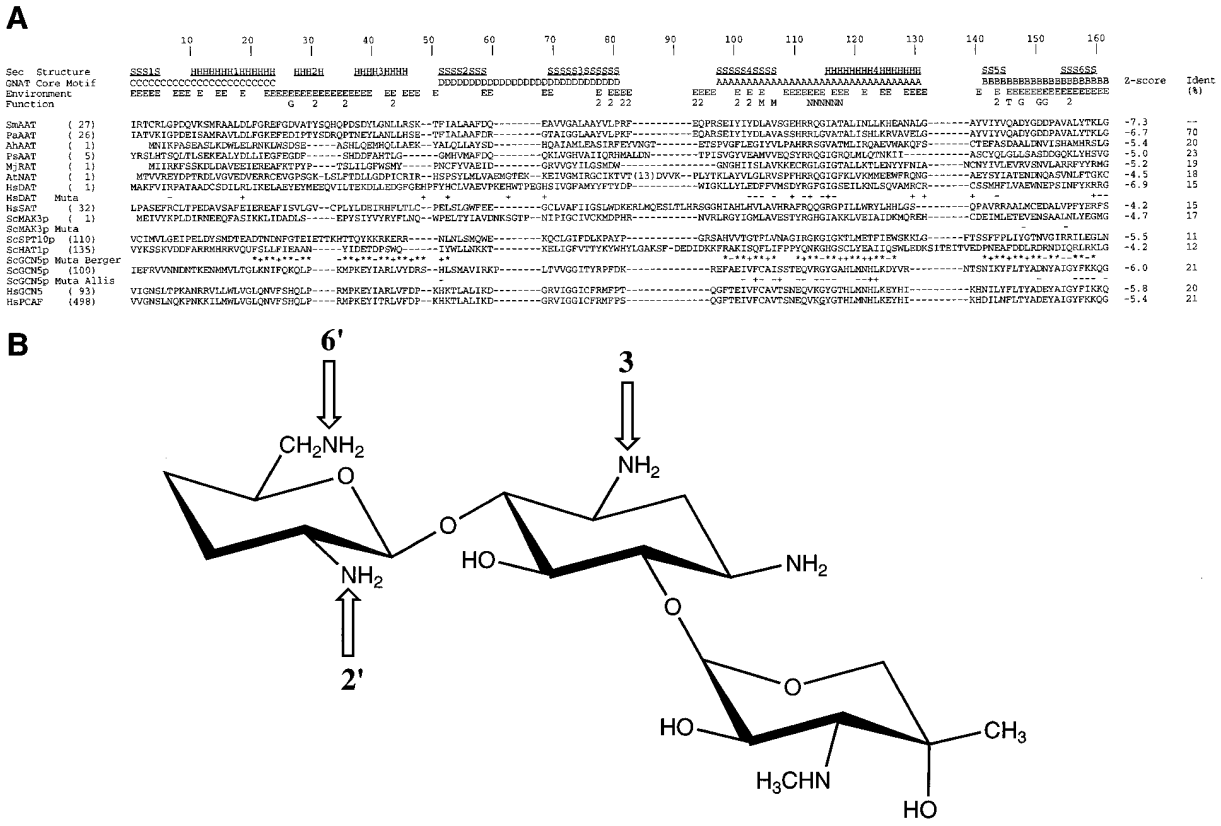

Figure 1. GCN5-Related N-acetyltransferases and Aminoglycoside Substrate

(A) Structure-based sequence alignment of GCN5-related N-acetyltransferases. The secondary structural elements were assigned from the X-ray structure (Kabsch and Sander, 1983), and the locations of GNAT motifs C, D, A, and B were obtained from the structure-based sequence alignments. Environment classification: E denotes residue with more than 20% of surface area accessible to solvent, calculated using MODELLER (Sali and Blundell, 1993). Functional classifications: N, main chain hydrogen bonds between amino groups and 3′-phosphate ADP; M, main chain hydrogen bonds between β-strand S5 and pantethenic acid; 2, contributes to dimer interface; T, Gln-145 acts as the threshold between the AcCoA-binding notch and the substrate-binding slot; G, acidic residues contributing to the negative electrostatic potential of the gentamicin-binding slot (Asp-53, Asp-147, Asp-150, Asp-151). Mutagenesis classification: -, point mutant with reduced activity; +, point mutant with little or no effect; *-*, multiple mutants with reduced activity. *+*, multiple mutants with little or no effect. Two sets of *Sc*GCN5p mutations are denoted Berger (Wang et al., 1998) and Allis (Kuo et al., 1998). Underlined Q and G in the *Hs*PCAF sequence denote sites of a double point mutation to glutamic acid that abolishes enzyme activity in vitro (data not shown). Sequence identities with *Sm*AAT and Z scores from the comparative modeling exercise are given for each structure-based alignment. Genbank accession codes: *Sm*AAT g239721, *Pa*AAT g150958, *Ah*AAT g455437, *Ps*AAT g625766, *Mj*RAT g1592161, *At*NAT g1277090, *Hs*DAT g36607, *Hs*SAT g1389592, *Sc*MAK3p g1314121, *Sc*SPT10p g402736, *Sc*HAT1p g965092, *Sc*GCN5p g417038, *Hs*GCN5 g1587472, *Hs*PCAF g1491937.

(B) Structure of gentamicin $C_{1\alpha}$, with arrows showing the three sites of acetyl group addition (3, 2′, and 6′).

polar side chain. Pantethenic acid binding is mediated by hydrogen bonds with main chain donors and acceptors. Motif B contributes acidic residues to the substrate-binding site, thereby neutralizing the positively charged aminoglycoside substrates. This work also serves as a foundation for directed mechanistic studies of members of the GCN5-related superfamily involved in regulation of eukaryotic gene expression.

Results and Discussion

Conserved Motifs A–D Constitute a Proteolytically Resistant GNAT Core

Mass spectrometry was performed after digestion of *Sm*AAT (in the absence of CoA) with two different sequence-specific proteases. This combination of classical biochemistry and high-resolution mass spectrometry has proved extremely useful for identifying globular domains within proteins (reviewed in Cohen, 1996). Most of the V8 protease and trypsin cleavage sites in *Sm*AAT map to its N and C termini (see Experimental Procedures). These data are compatible with the limits of the four conserved GNAT motifs (C, D, A, and B) identified by Neuwald and Landsman (1997), suggesting that the central portion of the enzyme corresponds to a protease-resistant phylogenetically conserved GNAT core (Figure 1). Additional, albeit indirect, support for this assertion comes from two sources. First, C-terminal truncation of *Sm*AAT beyond motif B yields wild-type gentamicin 3-N-acetyltransferase activity in vivo (see Experimental Procedures). Second, in our cocrystals the polypeptide chain is disordered outside the confines of the proteolytically resistant core defined by mass spectrometry (see Structural Overview).

Crystallization and Structure Determination

A truncated form of the enzyme (*Sm*AAT [1–168], which lacks nine dispensable C-terminal amino acids) plus

Table 1. Statistics of the Crystallographic Analysis

	Resolution (Å)	Reflections Measured/Unique	Completeness (%) Overall/Outer Shell	R_{sym} (%) Overall/Outer Shell	Phasing Power	
					Ano	Iso
MAD analysis (two Se sites)						
λ1 (0.9793 Å)	20.0–2.3	118,408/16,291	92.9/92.5	5.2/9.3	1.94	0.24
λ2 (0.9703 Å)	20.0–2.3	117,918/16,295	92.9/92.9	5.3/9.1	2.50	—
λ3 (0.9668 Å)	20.0–2.3	116,138/16,281	92.8/92.8	5.7/11.5	2.17	1.96
Overall figure of merit	0.58 acentric	0.38 centric				

Refinement Statistics (against λ1)

	Resolution (Å)	Completeness (%)	R factor	Free R factor
Data with $\|F\|>2\sigma(\|F\|)$	20.0–2.3	92.9	0.204	0.251
rms deviations	Bond lengths, 0.006 Å	Bond angles, 1.4°	Thermal parameters, 1.1 Å^2	

$r_{sym} = \Sigma|I-<I>|/\Sigma I$, where I = observed intensity, $<I>$ = average intensity obtained from multiple observations of symmetry related reflections.
Phasing power = rms ($|F_H|/E$), $|F_H|$ = heavy atom structure factor amplitude and E = residual lack of closure.
rms bond lengths and rms bond angles are the respective root-mean-square deviations from ideal values. rms thermal parameter is the root-mean-square deviation between the B values of covalently bonded atomic pairs.
Free R factor was calculated with 10% of data omitted from the structure refinement.

CoA yielded diffraction-quality cocrystals, which contain two crystallographically independent copies of the 1:1 protein–ligand complex in the asymmetric unit (see Experimental Procedures). The *Sm*AAT–CoA complex structure was determined via multiwavelength anomalous dispersion (Hendrickson, 1991) (Table 1). Experimental phases obtained at 2.3 Å resolution gave a high-quality electron density map that was improved by density modification and phase combination. The current refinement model has an R factor of 20.4% and a free R value of 25.1% (Brünger, 1992) at 2.3 Å resolution.

Structural Overview

The three-dimensional structure of *Sm*AAT is illustrated schematically in Figure 2. The single domain α/β fold encompasses the four conserved GNAT motifs (C, D, A, and B) and is shaped like a right hand wrapped around a narrow cylinder (α helix) with the "thumb" extending away from the cylinder (overall dimensions 37 Å [width] × 48 Å [height] × 40 Å [depth]). Secondary structural elements include three short and one long α helices and a six-stranded β sheet of mixed polarity, arranged in the order S1-H1-H2-H3-S2-S3-S4-H4-S5-S6. The six β strands are arranged in space in the order S1-S2-S3-S4-S5-S6, making a highly curved β sheet (Figures 2A and 2B). The three short α helices (H1, H2, and H3) meander across the convex surface of the β sheet (Figures 2B–2D). The ligand-binding cleft (AcCoA-binding notch) is generated by approximation of the concave surface of the β sheet to the long α helix (H4) (Figure 2).

To the best of our knowledge, the structure of *Sm*AAT represents a new protein fold. A search using the Dali server (Holm and Sander, 1993) revealed a maximum Z score of 3.3, obtained with a fragment of an unrelated α/β protein (β-galactosidase, PDB accession code 1BGL-A). Individual comparisons of *Sm*AAT with more than a dozen CoA-binding proteins (reviewed in Engel and Wierenga, 1996) reveals that *Sm*AAT is a novel member of this diverse protein family. As such, it represents a useful, long-awaited paradigm for structure-based sequence comparisons of the GNATs (see below).

Figures 2A–2D illustrate the structural roles played by each of the four motifs in the GCN5-related N-acetyltransferase core. Knowledge of the structure of a GNAT superfamily member allowed us to revise the definitions of the four conserved motifs, initially characterized by Neuwald and Landsman (1997). They now conform to the secondary structural boundaries and sequence conservation patterns in the structure-based alignment illustrated in Figure 1. Motif C corresponds to β-strand S1, the S1/H1 loop, and α helix H1 (color coded red), which contribute to the domain's hydrophobic core. Motif D forms a β hairpin (S2, the S2/S3 loop, and S3; color coded green). This segment of the polypeptide chain lies in the middle of the hydrophobic core between α helices H1 (motif C; red) and H4 (motif A; blue), making the GNAT core intolerant of nonconservative substitutions in motif D. Motif A is the most highly conserved of the four GNAT motifs. As predicted (Lu et al., 1996), motif A adopts a βα conformation (S4, the S4/H4 loop, and H4; color coded blue), and the invariant segment constitutes a significant portion of the AcCoA-binding site (see below). Finally, motif B corresponds to a β hairpin (S5, the S5/S6 loop, and S6; color coded magenta). This segment of the polypeptide chain forms the thumb-like structure of the GNAT core, lying at the edge of the six-stranded β sheet and making up part of the active site. It is remarkable that the amino acid side chains of residues 146–151 in motif B are not well defined in either half of the asymmetric unit, and these residues may interact with antibiotic substrates (see below).

Noncrystallographic Symmetry

The two *Sm*AAT–CoA complexes comprising the crystallographic asymmetric unit are related by a noncrystallographic 2-fold rotation (Figure 3). The structures are very similar, with root-mean-square (rms) deviations between α-carbon atomic positions of 0.3 Å, which is comparable to the error of the crystallographic method at 2.3 Å resolution (Brünger, 1998). Packing interactions between the proteins are mediated by salt bridges, hydrogen bonds, and van der Waals interactions, which bury more than 880 Å^2 of solvent-accessible surface area (Lee and Richards, 1971). The most remarkable feature of this dimeric structure is the 12-stranded β barrel created by 2-fold noncrystallographic symmetry (Figure 3B). The interior of the barrel is packed with a

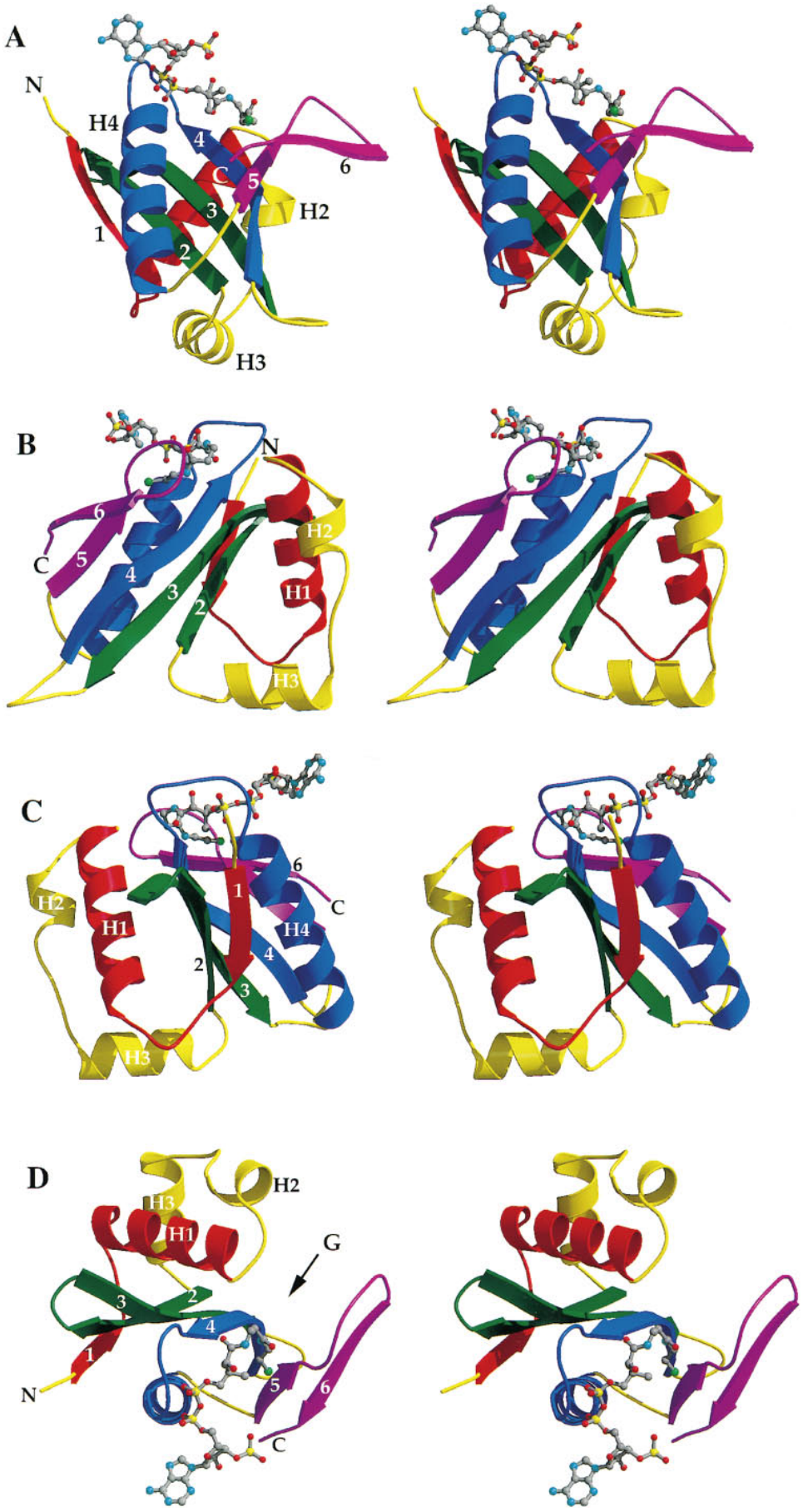

Figure 2. Structure of the *Sm*AAT–CoA Complex

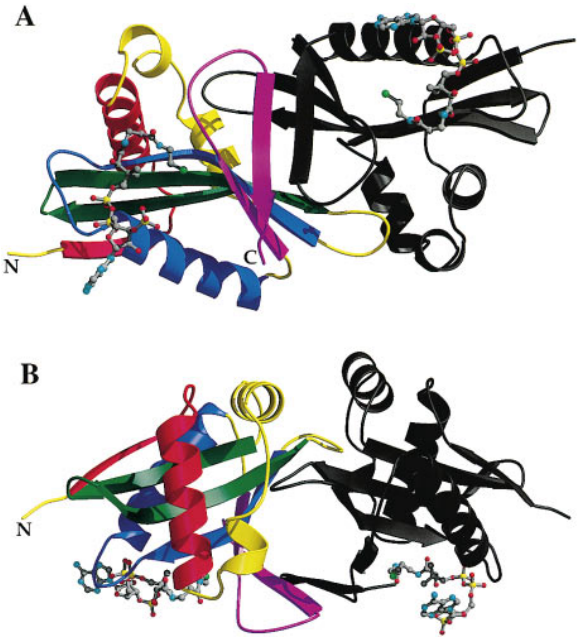

Figure 3. Structure of the *Sm*AAT Dimer in the Asymmetric Unit

(A) MOLSCRIPT/RASTER3D drawing viewed along the noncrystallographic 2-fold axis, showing the relative disposition of the two active sites. Complex 1 is illustrated and labeled with the scheme used in Figure 2, and complex 2 is shown in black. The conformational heterogeneity of the base, ribose, and 3′-phosphate are readily seen in this view.

(B) Drawing viewed at right angles to the noncrystallographic 2-fold axis, showing the 12-stranded β-barrel structure.

large number of aromatic residues, suggesting that the dimer is primarily stabilized by van der Waals interactions (see Figure 1 for residues buried on dimer formation). Two lines of evidence suggest that the enzyme exists as a dimer under physiologic conditions. First, the surface area buried (880 Å^2) exceeds 600 Å^2, which is the accepted upper limit for adventitious crystal-packing contacts (Janin, 1995). Second, a related enzyme, human spermidine/spermine NAT, has been shown to act as a dimer (Coleman et al., 1996). To date, we have not obtained conclusive hydrodynamic evidence that *Sm*AAT functions as a dimer. We have, however, shown that recombinant ovine serotonin NAT is a dimer at a concentration of about 1 mg/ml using dynamic light scattering (data not shown).

Sequence Alignments of Representative Aminoglycoside N-acetyltransferases

*Sm*AAT is very similar (70% identical) to its functional homolog isolated from *Pseudomonas aeruginosa* (*Pa*AAT) (Schwocho et al., 1995) but substantially less similar to an aminoglycoside 2′-N-acetyltransferase from *Providencia stuartii* (*Ps*AAT) (Rather et al., 1993) and an aminoglycoside 6′-N-acetyltransferase from *Acinetobacter hemolyticus* (*Ah*AAT) (Lambert et al., 1993). Amino acid sequence identities are 23% and 20%, respectively. Analysis of their respective GNAT core regions reveals that 30% of *Sm*AAT's core residues are either identical (8/136) or chemically similar (33/136) among the four AATs (Figure 1). Only *Pa*AAT has sufficient amino acid identity with *Sm*AAT to permit us to infer directly that it is a structural homolog of *Sm*AAT (Sander and Schneider, 1991). However, structure-based sequence alignments, three-dimensional model building, and evaluation of the resulting models provide us with a quantitative approach to the problem of detecting and confirming structural similarity in the face of relatively low pairwise amino acid identity.

Figure 1 illustrates the results of structure-based sequence alignments of *Ps*AAT and *Ah*AAT with *Sm*AAT. In addition, a Z score (Sippl, 1993) is reported for each homology model, giving a measure of the validity of the sequence alignment from which the model was derived. This measure depends on whether amino acid side chains have chemically appropriate environments in the corresponding model. The Z-score statistic permits direct comparison with the results of X-ray crystallography. For reference, typical Z scores for experimentally determined protein structures fall between −5 and −8, and the Z score for the structure of *Sm*AAT itself is −7.3. In contrast, random modeling exercises with unrelated proteins yield a mean Z score of 0 with a standard deviation of 1. How do the Z scores obtained for *Pa*AAT, *Ah*AAT, and *Ps*AAT compare? In each case, the Z score obtained from the modeling exercise (ranging from −5.0 to −6.7) is comparable to that of an experimentally determined X-ray or NMR structure and well outside the range of values typical for patently incorrect models. We conclude, therefore, that all three enzymatically distinct AATs (3, 2′, and 6′) are structural homologs, making our X-ray results useful for directed mechanistic studies of N-acetyltransferase–mediated aminoglycoside resistance. The only significant differences between the crystal structure of *Sm*AAT and the homology models of *Ah*AAT and *Ps*AAT occur between GNAT motifs C and D. Both structure-based sequence alignments predict deletions in this region, suggesting that the precise trajectory of the polypeptide chain from the C terminus of α-helix H1 to the N terminus of β-strand S2 is not conserved among distinct AATs.

Structure of *Sm*AAT-Bound Coenzyme A

The structure of *Sm*AAT-bound CoA is illustrated in Figure 4 (CoA atom names appear in italics). The electron

(A) MOLSCRIPT/RASTER3D (Kraulis, 1991; Merrit and Murphy, 1994) stereo drawing showing the concave surface of *Sm*AAT. CoA, included as an atomic stick figure, is located in the coenzyme-binding notch between the long α helix and the β sheet. α helices are labeled H1-H4, and β strands are labeled 1–6, with the N and C termini of the protein labeled with N and C, respectively. GNAT motifs C, D, A, and B are colored red, green, blue, and magenta, respectively.

(B) Stereo drawing viewed along the face of the β sheet, showing *Sm*AAT in profile, the entire coenzyme-binding notch, and the location of the three α helices on the molecule's convex dorsal surface.

(C) Stereo drawing viewed along the face of the β sheet, showing the location of the three α helices on the molecule's convex dorsal surface.

(D) Stereo drawing viewed from the upper surface of enzyme looking into the active site. G denotes the gentamicin-binding slot.

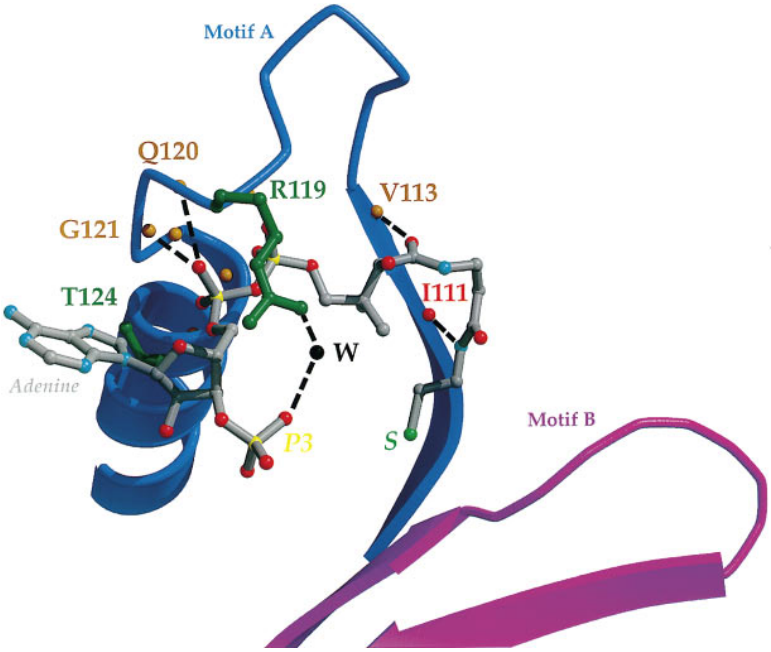

Figure 4. CoA Binding to *Sm*AAT

MOLSCRIPT/RASTER3D drawing of CoA in the coenzyme-binding notch of *Sm*AAT, showing selected residues involved in CoA recognition. A subset of the hydrogen bonds is indicated with dotted lines. The bulk of the hydrogen bonds with the 3′-phosphate ADP moiety and the bridging water molecule have been omitted for clarity. This view is similar to that shown in Figure 2D.

density for the ligand is well defined in both halves of the asymmetric unit (data not shown). Although the adenines, ribose sugars, and solvent-exposed 3′-phosphates differ somewhat between the two crystallographically independent complexes (Figure 3A), the remainder of the cofactors are very similar (rmsd between equivalent atoms = 0.2 Å). The ligand is bound to *Sm*AAT in a bent conformation with two quite different glycosyl *C1′-N* linkage torsion angles (χ = 84° and 12°) and *C2′-endo* ribose conformations. A bend occurs in the middle of the pantetheine arm, bringing the sulfur atom of the β-mercapto-ethylamine moiety close to the entrance to the AcCoA-binding notch. This ligand conformation is similar to those observed for CoA interacting with enoyl-CoA hydratase, citrate synthetase, and Acyl-CoA binding protein (PDB Codes: 1DUB, 2CTS, and 1ACA). However, the majority of bound CoA structures show an extended pantetheine conformation (PDB Codes: 1EAB, 1BUC, 3MDE, 1SCU, and 1REQ).

Coenzyme A Binding

The structure of the *Sm*AAT-CoA complex represents the ninth example of an enzyme bound to this cofactor (for a comprehensive review of protein–CoA complex structures, see Engel and Wierenga, 1996). Although their crystal lattice environments are not the same, the two crystallographically independent *Sm*AAT–CoA complexes make similar protein–ligand interactions, burying portions of both the protein and CoA surfaces (total solvent-accessible surface area of the protein buried by one CoA molecule = 110 Å^2). An electron density feature corresponding to one well-ordered water molecule was found between the protein and the ligand. This bridging water is common to both complexes, participating in a similar hydrogen bond network between the protein and the CoA (see below). As in all previously published enzyme–CoA cocrystal structures, the 3′-phosphate groups are solvent exposed, adopting different positions in the two halves of the asymmetric unit. In complex 1, the 3′-phosphate group participates in a water-mediated interaction with Arg-119 (NH1—H_2O = 2.3 Å and H_2O—*O32* = 3.0 Å); whereas, in complex 2 Arg-119 interacts directly with a 3′-phosphate oxygen atom (NH1—*O32* = 2.8 Å). It is remarkable that neither adenine base makes direct interactions with the enzyme, distinguishing *Sm*AAT from most CoA-binding proteins.

The remainder of the CoA structure is well ordered and interacts with the invariant Arg/Gln-X-X-Gly-X-Gly/Ala segment (the S4/H4 loop and the N terminus of α-helix H4) plus the C-terminal portion of β-strand S4, both of which are derived from GNAT motif A. The negatively charged diphosphate moiety is held in the AcCoA-binding notch (Figures 4 and 5) by contacts with multiple backbone NH groups, the side chain of Thr-124 and a bridging water molecule (denoted BW). Protein–cofactor interactions include the following: Thr-124 OG1—*O11* = 2.7 Å, Thr-124 N—*O11* = 3.0 Å, Ala-123 N—*O11* = 3.2 Å, Ala-123 N—*O21* = 2.7 Å, Ile-122 N—*O11* = 3.4 Å, Ile-122 N—BW = 2.9 Å, Gly-121 N—*O12* = 2.7 Å, Gly-121 N—BW = 2.9 Å, Gln-120 N—*O12* = 3.2 Å, Gln-120 N—BW = 2.7 Å, BW—*O21* = 3.0 Å, BW—*O22* = 3.0 Å, and Arg-119 N—*O22* = 2.6 Å. Direct protein–ligand contacts occur between motif A and the pantethenic acid, including Val-113 N—*OP6*= 2.8 Å and Leu-111 O—*NP1* = 2.8 Å. Two of the three remaining hydrogen bonding functionalities in the pantethenic acid are solvent accessible and interact with water molecules (*OP3*—H_2O = 2.7 Å and *NP2*—H_2O = 3.3 Å). Finally, we cannot exclude contributions to AcCoA binding from motif B. The side chain of Asp-147 is not visible in the electron density map, but model building suggests that it could interact with *OP1* of pantetheine if the S5/S6 loop were better ordered.

A similar mode of 3′-phosphate ADP binding has been observed in the cocrystal structure of succinyl-CoA synthetase (Wolodko et al., 1994), which employs a βαβ

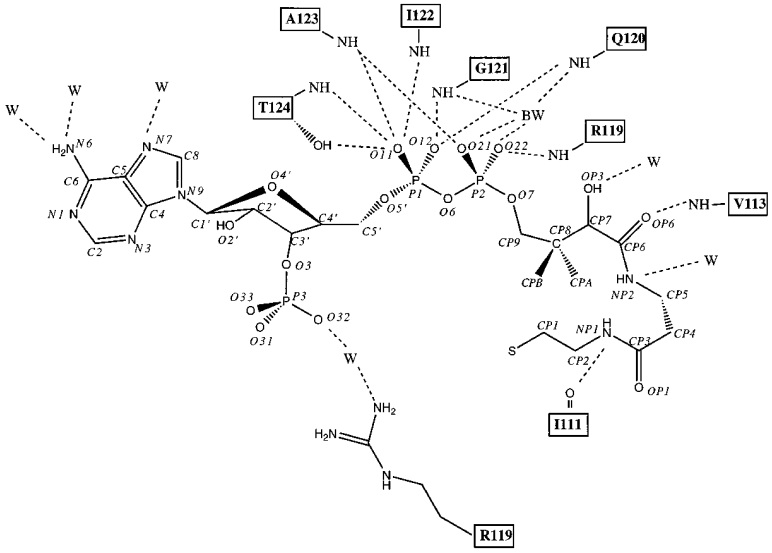

Figure 5. Schematic Drawing of CoA–*Sm*AAT Interactions

Dashed lines denote hydrogen bonds. Interatomic distances are listed in the text (see Coenzyme A Binding). The hydrogen bond between Ile22 N and the bridging water (BW) has been omitted for clarity.

Rossmann dinucleotide-binding fold (Rossmann et al., 1975). Although GNAT motifs A plus B in *Sm*AAT are superficially similar to a canonical Rossmann fold, they are not a perfect match, and the CoA chains in the succinyl-CoA synthetase and *Sm*AAT cocrystal structures actually point in opposite directions.

Structural Analysis of the *Sm*AAT Active Center

All AcCoA-dependent enzymes exploit the fact that the loosely bound acetyl group (attached to CoA by a relatively weak thioester linkage) can be transferred either to the enzyme (creating a covalent intermediate) and then onto the substrate, or in a single step directly to the substrate. Cole and coworkers have proposed an ordered BiBi ternary complex (sequential) kinetic mechanism for ovine serotonin NAT (De Angelis et al., 1998) that is probably common to all GNATs. Results of inhibition studies using recombinant enzyme and various AcCoA and serotonin analogs suggest that the reaction begins with AcCoA binding, followed by binding of serotonin, then direct transfer of the acetyl group from AcCoA to serotonin, followed by product and then CoA release. Williams and Northrop (1979) reached similar mechanistic conclusions using a bisubstrate analog inhibitor of gentamicin 3-N-acetyltransferase I from *Pseudomonas aeruginosa*, which is a functional homolog of *Sm*AAT.

Comparison of the sequences of *Sm*AAT, *Ps*AAT, and *Ah*AAT suggests that these three structurally similar but enzymatically distinct AATs probably bind cofactor using similar interactions between ligand and the polypeptide backbone. The 3′-phosphate ADP-binding residues comprising the S4/H4 loop and the N terminus of α-helix H4 show minimal variation (Arg-Arg-Gln/Ser-Gly-Ile/Val-Gly/Ala-Thr/Arg) among the three sequences, and the segments contributing to pantetheine binding are all hydrophobic (Leu-Ala-Val versus Ile-Tyr-Val and Met-Val-Val). Indirect support for this prediction comes from the results of site-directed mutagenesis of the invariant Arg/Gln-X-X-Gly-X-Gly/Ala segment in other GNAT superfamily members (see Introduction), and our homology modeling exercise, which showed no significant variation within motif A in any of the structural models (data not shown).

What additional insights does our cocrystal structure provide regarding enzyme-catalyzed acetylation of aminoglycoside antibiotics? In principle, the sulfur atom of CoA (*S* in Figure 4) should mark the precise location of the enzyme's active center, but it seems unlikely to do so in this case because the bent conformation of the pantetheine would place the active site in the vicinity of the 3′-phosphate. Steric considerations rule out this naive interpretation of our result, given the size of the aminoglycoside substrate. It seems likely that, in the absence of the acetyl group, the CoA has adopted a bent conformation. If AcCoA adopted an extended conformation, the acetyl group would lie above the side chain of Gln145 (data not shown), which forms part of the floor of the active site dividing the AcCoA-binding notch from the substrate-binding surface (Figure 6).

Inspection of the molecular surface in the vicinity of the AcCoA-binding notch reveals the features illustrated in Figure 6. Motif B provides a β-hairpin projection (S5, S5/S6 loop, and S6), previously referred to as the thumb. The S5/S6 loop creates one wall of a narrow canyon-like feature (Figure 6B) with negative electrostatic potential that extends away from the AcCoA-binding surface toward the convex face of the enzyme. The other wall is provided by the acidic H1/H2 loop. The resulting "gentamicin-binding slot," marked G in Figure 2D, could serve as a binding site for the polycationic aminoglycosides. Support for this assertion comes from our cocrystal structure, in which the putative gentamicin-binding slot is occupied by a positively charged spermidine molecule (data not shown). Thus, Asp-53 (from the H1/H2 loop) and Asp-147, Asp-150, and Asp-151 (from the S5/S6 loop) almost certainly contribute to substrate binding during acetylation of aminoglycosides by *Sm*AAT and related 3-N-acetyltransferases (e.g., *Pa*AAT in Figure 1). Sequence analyses and homology modeling of the 2′- and 6′-N-acetyltransferases (*Ps*AAT and *Ah*AAT in Figure 1) document that they also have negatively charged residues in their predicted H1/H2 and S5/S6 loops. It seems likely, therefore, that the three enzymatically distinct AATs use similar substrate binding strategies,

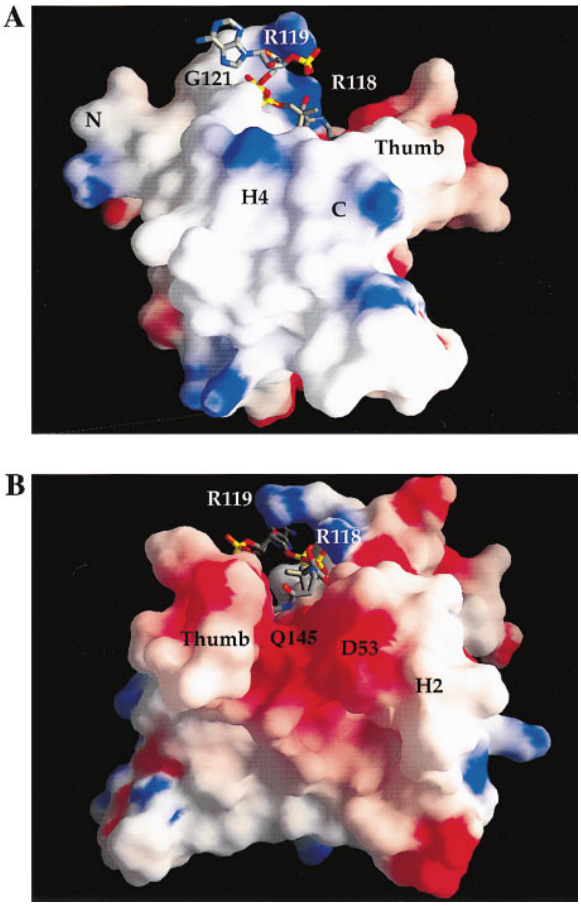

Figure 6. Surface Properties of *Sm*AAT

GRASP (Nicholls et al., 1991) representations of the chemical properties of the solvent-accessible surface of *Sm*AAT calculated using a water probe radius of 1.4 Å. The surface electrostatic potential is color coded red and blue, representing electrostatic potentials <-8 to $>+8$ k_BT, where k_B is the Boltzmann constant and T is the temperature. The calculations were performed with an ionic strength of 0 and dielectric constants of 80 and 2 for solvent and protein, respectively (Gilson et al., 1988).

(A) AcCoA-binding surface of *Sm*AAT, showing CoA in the cofactor-binding notch. The locations of selected residues involved in CoA recognition (Arg-118, Arg-119, and Gly-121) are labeled, with the N and C termini, α-helix H4, and the thumb-like structure. This view is identical to that shown in Figure 2A.

(B) Active site surface of *Sm*AAT, showing CoA in the cofactor-binding notch and the negatively charged gentamicin-binding slot, with the locations of Asp-53, Arg-118, Arg-119, Gln-145, α-helix H2, and the thumb-like structure. This view is similar to that shown in Figure 2B.

which exploit a narrow, negatively charged aminoglycoside-binding slot. Although it is tempting to go beyond descriptions of the AcCoA- and aminoglycoside-binding surfaces and try to make specific predictions about the catalytic roles of individual side chains, it is impossible to do so in the absence of structural data on binding of a bisubstrate analog inhibitor. Efforts are currently underway to prepare suitable cocrystals.

Sequence Alignments of Representative GNAT Superfamily Members

Figure 1 illustrates structure-based sequence alignments for *Sm*AAT and representative members of the GNAT superfamily, derived from an archaebacterium, a green plant, budding yeast, and human. These enzymes catalyze acetyl group addition to ribosomal protein S18 (*Methanococcus jannaschii* N-acetyltransferase, *Mj*NAT), a viral gag protein (*Saccharomyces cerevisiae* gag protein N-acetyltransferase, *Sc*MAK3p), basic histone tails (*S. cerevisiae* HAT1p, *Sc*HAT1p; *S. cerevisiae* GCN5p, *Sc*GCN5p; human GCN5, *Hs*GCN5; human PCAF, *Hs*PCAF), spermine or spermidine (human spermidine/spermine N1-acetyltransferase, *Hs*DAT), and serotonin (human serotonin N-acetyltransferase, *Hs*SAT), or represent putative N-acetyltransferases with no known substrates (*Arabidopsis thaliana* hookless1, *At*NAT; *S. cerevisiae* SPT10p, *Sc*SPT10p). Z scores for the models constructed with these structure-based alignments fall between -4.2 and -6.9, with most of the alignments yielding values of -4.7 or better. Our results strongly suggest that all of these proteins share a common GNAT core (ranging in length from 119 to 161 residues) that supports N-acetyltransferase activity. Moreover, this analysis provides additional evidence for the existence of a GNAT superfamily that evolved from a common ancestral NAT (Neuwald and Landsman, 1997). Corroboration of this assertion is provided by the results of site-directed mutagenesis of *Hs*DAT (Coleman et al., 1996; Lu et al., 1996) and *Sc*MAK3p (Tercero et al., 1992) (Figure 1). In *Hs*DAT, all but one of the alanine-scanning mutations affecting catalysis map to motifs A or B, where they could interfere with either AcCoA or substrate binding. Most of the mutations that had little or no effect map to the surface of the *Sm*AAT structure, where they would be tolerated. In *Sc*MAK3p, the two point mutations that inactivate the *mak3* gene map to motif B, where they could interfere with substrate binding. The Tyr130Ala mutation is particularly interesting because this conserved hydrophobic residue plays an important role in *Sm*AAT, stabilizing the structure of the motif B β-hairpin structure that contributes to the gentamicin-binding slot.

In the absence of a three-dimensional structure of a nuclear histone N-acetyltransferase (HAT), such as GCN5 or PCAF, our work provides a framework with which to examine how these biologically important enzymes modulate eukaryotic transcription (reviewed in Ogryzko et al., 1996; Grunstein, 1997; Wade et al., 1997; Mizzen and Allis, 1998; Struhl, 1998). The structure-based sequence alignments presented in Figure 1 suggest that the portions of yeast GCN5p, human GCN5, and human PCAF supporting N-acetyltransferase activity are structurally similar to *Sm*AAT. Z scores obtained from model building range between -5.4 and -6.0, which are comparable to Z scores calculated for experimentally determined X-ray and NMR structures. Further evidence that these eukaryotic HATs are related to our eubacterial AAT comes from the results of site-directed mutagenesis of yeast GCN5p (Kuo et al., 1998; Wang et al., 1998) and human PCAF (Yang et al., 1996; data not shown). Mutations reducing or abolishing nuclear histone activity map to the region between motifs C and D, and motifs A and B (Figure 1). Most of the deleterious substitutions mapping to the N-terminal half of *Sm*AAT can be readily explained, because they imply changes in one or more buried residues that could destabilize the structure of the hydrophobic core. The most clear cut example is

His-145 in yeast GCN5, which corresponds to a buried phenylalanine in *Sm*AAT. In motifs A and B, the bulk of the mutations reducing activity map to AcCoA-binding residues or motif B, where they could influence substrate binding and catalysis.

The structure-based alignments of *At*NAT, *Hs*SAT, and *Sc*HAT1p are somewhat less satisfactory (Z scores range between −4.2 and −4.5) than for the other representative members of the GNAT superfamily (Z scores of −4.7 or better). Inspection of the homology models revealed that these relatively low Z scores result from predicted deletions between motifs C and D and insertions between motifs D and A. It is, therefore, probable that the structures of these three enzymes differ from our cocrystal structure in two short regions. First, the connection between the C terminus of α-helix H1 and the N terminus of β-strand S2 is likely to be random coil instead of the combination of α helices H2 and H3 and random coil in *Sm*AAT. Second, the S3/S4 loop would be predicted to be longer in all three enzymes, with the longest loop expected to occur in *At*NAT.

Conclusion

The three-dimensional structure of this novel antibiotic-resistance enzyme explains acetyl coenzyme A binding and identifies the location of putative active-site residues responsible for recognition of gentamicin and other aminoglycoside antibiotics. Our work also provides the structure of the GCN5-related N-acetyltransferase core, which represents a starting point for further crystallographic, biochemical, and genetic studies of members of a large superfamily of N-acetyltransferases that catalyze acetyl group addition in various biologically important contexts. In particular, these results should aid directed, systematic analyses of the mechanisms by which the histone N-acetyltransferases neutralize selected positively charged lysine residues in the N-terminal tails protruding from the body of the histone octamer, affecting DNA packaging and transcription in eukaryotes.

Experimental Procedures

Protein Preparation and Crystallization

Full-length *Serratia marcescens* aminoglycoside-3-N-acetyltransferase (*Sm*AAT[1–177], GenBank accession code g239721) fused with an additional 21 N-terminal amino acids (MGSSHHHHHHSSGE NLYFQGH) was expressed in *E. coli* and purified via Ni^{2+}-ion affinity chromatography (Nikolov et al., 1992). Mass spectrometry documented that a significant portion of the purified *Sm*AAT was proteolyzed, yielding a mixture of full-length protein plus a C-terminal truncation beyond residue 168 (data not shown). This material was deemed to be unsuitable for crystallization. Reasoning that flexibility of the C-terminal portion of the protein was responsible for its removal, we expressed and purified the appropriate truncation [*Sm*AAT(1–168)]. Tobacco etch virus protease was used to remove the bulk of the hexa-histidine tag, leaving two amino acids Gly and His N-terminal to the initiation Met of *Sm*AAT. The measured molecular mass for *Sm*AAT (1–168) was 18,630 ± 60 (predicted 18,649). Proteolysis combined with mass spectrometry revealed sites within *Sm*AAT (1–168) that are exquisitely sensitive to trypsin (Arg-3, Arg-14, Lys-16, and Lys-18), suggesting that the N terminus of the enzyme is also disordered. Lower efficiency protease cleavage sites near the C terminus of this truncated form of *Sm*AAT include Glu-165 (V8 protease) and Lys-159 and Arg-163 (trypsin). Crystallization trials with *Sm*AAT(1–168) plus CoA yielded crystals in the monoclinic space group C2 (a = 78.5 Å, b = 102.3 Å, c = 50.1 Å, β = 93.7°), with two protein–ligand complexes in the asymmetric unit that diffract to at least 2.0 Å resolution. *Sm*AAT(1–168)-CoA cocrystals were grown by sitting-drop vapor diffusion at 4°C with a protein concentration of 3.5 mg/ml and 5 mM CoA against a reservoir containing 100 mM Tris-HCl (pH 7.8), 0.8% PEG 4K, 18% *t*-butanol, 20 mM $SrCl_2$, 7% dioxane, 5% 2,4-methylpentanediol, 40 mM hexanediol, 10 mM dithiothreitol, 2 mM tri(2-carboxyethyl)phosphine-HCl, 10 mM spermidine, and 2.5% glycerol. As a precaution to ensure ligand binding, the protein was incubated with CoA for approximately 30 min prior to crystallization trials. A similar protocol is currently being used to prepare cocrystals with AcCoA. *Sm*AAT(1–168) was also expressed in its selenomethionine (Se-Met) substituted form, and the Se-Met protein was purified and crystallized as above. Crystal cryoprotection was achieved by adding glycerol to a final concentration of 17% plus 8% *2R,3R*-butanediol. More conventional cryoprotection regimes prevented ice formation but showed substantial increases in crystal mosaic spread (>1°). Regrettably, attempts to cocrystallize *Sm*AAT with both CoA and gentamicin were complicated by a dramatic reduction in enzyme solubility and were not successful. Crystal soaking experiments with gentamicin were similarly unsuccessful.

Antibiotic Resistance Assay

*Sm*AAT activity was determined by evaluating gentamicin resistance of *E. coli* transformed by a plasmid encoding the *aat* gene. A 1325 base pair BamHI-MscI fragment including the *aat* gene was isolated from pFastBac1 (Life Technologies) and subcloned into pBluescript KS(-) (Stratagene) digested with BamHI and EcoRV. To test the activity of the C-terminal truncation of *Sm*AAT, a stop codon was introduced after the codon corresponding to His-168 by in vitro mutagenesis. The resulting plasmids encoding wild-type and truncated *Sm*AAT, plus the empty vector as a negative control, were introduced into *E. coli* DH5α. Gentamicin resistance was assessed by growing the transformed *E. coli* on LB agar plates with various concentrations of the antibiotic (0, 0.1, 0.3, 1, 3, 10, 20, 30, and 60 μg/ml) for 24 hr. At 0.3 μg/ml, growth of bacteria containing the empty vector was completely inhibited. *E. coli* harboring the plasmids encoding either the wild-type or truncated enzymes were both resistant to gentamicin up to a concentration of 20 μg/ml, documenting that truncation of *Sm*AAT does not affect enzyme activity in vivo.

Data Collection, Structure Determination, and Refinement

Se-Met multiwavelength anomalous dispersion data (Hendrickson, 1991) were collected at −160°C on the CHESS F2 beamline, using reverse-beam geometry to record Friedel pairs at three X-ray wavelengths, corresponding to one remote point above the Se absorption edge (λ_3) and the absorption edge inflection point (λ_1) and peak (λ_2). Data were processed using MOSFLM (Leslie, 1990). Two of the possible eight selenium sites were found using Patterson syntheses. The remaining methionine residues occur within disordered regions of the protein and were never visualized. Experimental phases (α_{MAD}) were estimated at 2.3 Å resolution using SHARP (de La Fortelle and Bricogne, 1997), giving final figures of merit of 0.58 and 0.38 for acentric and centric reflections, respectively. The resulting $|F_{observed}|/\alpha_{MAD}$ Fourier map showed good contrast between solvent and protein regions, with right-handed α helices and β strands clearly visible. After density modification using SOLOMON (Abrahams and Leslie, 1996), virtually all of the ordered residues were built into the high-quality electron density map (Jones et al., 1991). Model building interspersed with positional, simulated annealing and temperature factor refinement using CNS (Brünger et al., 1998) permitted location of coenzyme and an unambiguous trace and sequence assignment of *Sm*AAT. It is remarkable that only two selenium atoms were responsible for phasing 273 residues plus two copies of CoA, which is somewhat higher than the recommended ratio of 90 residues per selenium atom derived from Hendrickson (1991).

The current refinement model consists of *Sm*AAT residues 25–161 plus CoA (complex 1), and *Sm*AAT residues 25–160 plus CoA (complex 2), plus 253 hydration waters and one spermidine molecule. The electron density for the polypeptide backbone is everywhere continuous at 1.3 σ in a $(2|F_{observed}|-|F_{calculated}|)$ difference Fourier synthesis, except between residues 146–151 where breaks occur. In complex 1 there is continuous electron density for the backbone

atoms for residues 146–150 but no clear side chain density for Asp-147, Tyr-148, and Asp-151. All illustrations of *Sm*AAT are derived from complex 1. The portions of the polypeptide chain that were not included in the refinement correspond well with the results of proteolysis/mass spectrometry (see above), which also showed a low efficiency cleavage by V8 protease at Asp-147. The two CoA molecules are well defined in the electron density map. PROCHECK (Laskowski et al., 1993) revealed no unfavorable (ϕ, ψ) combinations, and main chain and side chain structural parameters consistently better than those expected at 2.3 Å resolution (overall G factor = 0.3). Average B factors are 23 Å^2 and 37 Å^2 for protein atoms and water molecules, respectively.

Structure-Based Sequence Alignments

Twelve broadly representative GNAT sequences plus the sequence of a functional homolog of *Sm*AAT from *Pseudomonas aeruginosa* (Schwocho et al., 1995) were selected for structure-based sequence alignment using *Sm*AAT. The alignments reported by Neuwald and Landsman (1997) were manually edited based on the secondary and tertiary structures of *Sm*AAT. These improved sequence alignments were used to generate three-dimensional models based on the *Sm*AAT structure via a fully automated procedure implemented in MODELLER (Sali and Blundell, 1993). The models were evaluated using empirical energy scores generated by PROSAII (Sippl, 1993). This model evaluation program indicated both global and local problems with particular alignments. Such problematic cases were manually adjusted, and then model building and evaluation procedures were repeated. This cycle of alignment, model building, and evaluation was repeated several times for some sequences. Such an iterative procedure has proved useful for resolving a variety of challenging alignment problems (Sanchez and Sali, 1997). The overall reliability of the final structure-based alignments of SmAAT with 13 target sequences and the overall quality of the corresponding three-dimensional models are illustrated by pairwise sequence identities and model Z scores (Figure 1).

Acknowledgments

At CHESS we thank Dr. Dan Thiel and the MacCHESS staff for their help using Beamline F2. We thank Drs. J. Bonanno, J. Marcotrigiano, and S. K. Nair for their invaluable assistance with X-ray measurements and figure preparation, and Drs. V. G. Allfrey, B. T. Chait, S. L. Cohen, K. Gajiwala, D. Jeruzalmi, J. Kuriyan, H. Lewis, G. A. Petsko, R. G. Roeder, and A. Tomasz for useful discussions. S. K. B. is an Investigator in the Howard Hughes Medical Institute. This work was supported in part by the Rockefeller University and Richard M. and Isabel P. Furland (S. K. B.). E. W. is a Deutscher Akademischer Austauschdienst Fellow. A. S. is a Sinsheimer Scholar and an Alfred P. Sloan Research Fellow and is supported by the National Institutes of Health (GM54762) and the National Science Foundation (BIR-9601845).

Received July 2, 1998; revised July 17, 1998.

References

Abrahams, G.P., and Leslie, A.G.M. (1996). Methods used in the structure determination of F1 ATPase. Acta Crystallogr. *D52*, 30–42.

Allfrey, V.G., Faulkner, R., and Mirsky, A.E. (1964). Acetylation and methylation of histones and their possible role in the regulation of RNA synthesis. Proc. Natl. Acad. Sci. USA *51*, 786–794.

Brünger, A.T. (1992). Free R value: a novel statistical quantity for assessing the accuracy of crystal structures. Nature *355*, 472–475.

Brünger, A.T. (1998). Free R value: cross-validation in crystallography. Methods Enzymol. *277*, 366–396.

Brünger, A., Adams, P.D., Clore, G.M., Gros, P., Grosse-Kuntsleve, R.W., Jiang, J.-S., Kuszewski, J., Nilges, M., Pannu, N.S., and Read, R.J. (1998). Crystallography and NMR system: a new software system for macromolecular structure determination. Acta Crystallogr. D, in press.

Cohen, S.L. (1996). Domain elucidation by mass spectrometry. Structure *4*, 1013–1016.

Coleman, C.S., Huang, H., and Pegg, A.E. (1996). Structure and critical residues at the active site of spermidine/spermine N^1-acetyltransferase. Biochem. J. *316*, 697–701.

De Angelis, J., Gastel, J., Klein, D.C., and Cole, P.A. (1998). Kinetic analysis of the catalytic mechanism of serotonin N-acetyltransferase (EC 2.3.1.87). J. Biol. Chem. *273*, 3045–3050.

de La Fortelle, E., and Bricogne, G. (1997). Maximum-likelihood heavy atom parameter refinement for multiple isomorphous replacement and multiwavelength anomalous diffraction methods. Methods Enzymol. *276*, 472–494.

Engel, C., and Wierenga, R. (1996). The diverse world of coenzyme A binding proteins. Curr. Opin. Struct. Biol. *6*, 790–797.

Gilson, M., Sharp, K., and Honig, B. (1988). Calculating the electrostatic potential of molecules in solution: method and error assessment. J. Comput. Chem. *9*, 327–335.

Grunstein, M. (1997). Histone acetylation in chromatin structure and transcription. Nature *389*, 349–352.

Hendrickson, W. (1991). Determination of macromolecular structures from anomalous diffraction of synchrotron radiation. Science *254*, 51–58.

Hilfiker, A., Hikfiker-Kleiner, D., Pannuti, A., and Lucchesi, J.C. (1997). *mof*, a putative acetyl transferase gene related to Tip60 and MOZ human genes and the SAS genes of yeast, is required for dosage compensation in *Drosophila*. EMBO J. *16*, 2054–2060.

Holm, L., and Sander, C. (1993). Families of structurally similar proteins, version 1.0. J. Mol. Biol. *233*, 123–138.

Janin, J. (1995). Principles of protein-protein recognition from structure to thermodynamics. Biochimie *77*, 497–505.

Javier Teran, F., Alvarez, M., Suarez, J.E., and Mendoza, M.C. (1992). Characterization of two aminoglycoside-3-N-acetyltransferase genes and assay as epidemiological probes. Antimicrob. Chemotherapy *28*, 333–346.

Jones, T.A., Zou, J.Y., Cowan, S.W., and Kjeldgaard, M. (1991). Improved methods for building protein models in electron density maps and the location of errors in these models. Acta Crystallogr. *A47*, 110–119.

Kabsch, W., and Sander, C. (1983). Dictionary of protein secondary structure: pattern recognition of hydrogen-bonded and geometrical features. Biopolymers *22*, 2577–2637.

Kraulis, P.J. (1991). MOLSCRIPT: a program to produce both detailed and schematic plots of protein structures. J. Appl. Crystallogr. *24*, 946–950.

Kuo, M.-H., Zhou, J., Jambeck, P., Churchill, M.E.A., and Allis, C.D. (1998). Histone acetyltransferase activity of yeast Gcn5p is required for the activation of target genes in vivo. Genes Dev. *12*, 627–639.

Lambert, T., Gerbaud, G., Galimand, M., and Courvalin, P. (1993). Characterization of the *Acinetobacter hemolyticus* aac(6′)-Ig gene encoding an aminoglycoside 6′-N-acetyltransferase which modifies amikacin. Antimicrob. Agents Chemother. *37*, 2093–2100.

Laskowski, R.J., MacArthur, M.W., Moss, D.S., and Thornton, J.M. (1993). PROCHECK: a program to check stereochemical quality of protein structures. J. Appl. Crystallogr. *26*, 283–290.

Lee, B., and Richards, F.M. (1971). The interpretation of protein structures: estimation of static accessibility. J. Mol. Biol. *55*, 379–400.

Leslie, A.G.W. (1990). Crystallographic Computing. (Oxford: Oxford University Press).

Lu, L., Berkey, K.A., and Casero, R.A.J. (1996). RGFGIGS is an amino acid sequence required for acetyl coenzyme A binding and activity of human spermidine/spermine N^1-acetyltransferase. J. Biol. Chem. *271*, 18920–18924.

Merrit, E., and Murphy, M. (1994). Raster 3D version 2.0: a program for realistic molecular graphics. Acta Crystallogr. *D50*, 869–873.

Miller, G.H., Sabatelli, F.J., Hare, R.S., Glupczynski, Y., Mackey, P., Shales, D., Shimizu, K., and Shaw, K.J. (1997). The most frequent aminoglycoside resistance mechanisms—changes with time and geographic area: a reflection of aminoglycoside usage patterns? Clin. Infect. Dis. *24*, S46-S62.

Mizzen, C.A., and Allis, C.D. (1998). Linking histone acetylation to transcriptional regulation. Cell Mol. Life Sci. *54*, 6–20.

Neuwald, A.F., and Landsman, D. (1997). GCN5-related N-acetyltransferases belong to a diverse superfamily that includes the yeast SPT10 protein. Trends Biochem. Sci. *22*, 154–155.

Nicholls, A., Sharp, K., and Honig, B. (1991). Protein folding and association: insights from the interfacial and thermodynamic properties of hydrocarbons. Proteins Struct. Funct. Genet. *11*, 281–296.

Nikolov, D.B., Hu, S.-H., Lin, J., Gasch, A., Hoffmann, A., Horikoshi, M., Chua, N.-H., Roeder, R.G., and Burley, S.K. (1992). Crystal structure of TFIID TATA-box binding protein. Nature *360*, 40–46.

Ogryzko, V.V., Schiltz, R.L., Russanova, V., Howard, B.H., and Nakatani, Y. (1996). The transcriptional coactivators p300 and CBP are histone acetyltransferases. Cell *87*, 953–959.

Rather, P.N., Orosz, E., Shaw, K.J., Hare, R., and Miller, G. (1993). Characterization and transcriptional regulation of the 2′-N-acetyltransferase gene from *Providencia stuartii*. J. Bacteriol. *175*, 6492–6498.

Rossmann, M.G., Liljas, A., Branden, C.I., and Banaszak, L. (1975). Evolutionary and structural relationships among dehydrogenases. In The Enzymes, P.D. Boyer, ed. (New York: Academic Press), pp. 61–102.

Sali, A., and Blundell, T.L. (1993). Comparative protein modeling by satisfaction of spatial restraints. J. Mol. Biol. *234*, 779–815.

Sanchez, R., and Sali, A. (1997). Evaluation of comparative protein structure modelling by MODELLER-3. Proteins Struct. Funct. Genet. Suppl. *1*, 50–58.

Sander, C., and Schneider, R. (1991). Database of homology-derived protein structures and structural meaning of sequence alignment. Proteins Struct. Funct. Genet. *9*, 56–68.

Schwocho, L.R., Schaffner, C.P., Miller, G.H., Hare, R.S., and Shaw, K.J. (1995). Cloning and characterization of a 3-N-aminoglycoside acetyltransferase gene, aac(3)-Ib, from *Pseudomonas aeruginosa*. Antimicrob. Agents Chemother. *39*, 1790–1796.

Shaw, K.J., Rather, P.N., Hare, R.S., and Miller, G.H. (1993). Molecular genetics of aminoglycoside resistance genes and familial relationships of the aminoglycoside-modifying enzymes. Microbiol. Rev. *57*, 138–163.

Sippl, M. (1993). Recognition of errors in three-dimensional structures of proteins. Proteins Struct. Funct. Genet. *17*, 355–362.

Smith, E.R., Eisen, A., Gu, W., Sattah, M., Pannuti, A., Zhou, J., Cook, R.G., Lucchesi, J.C., and Allis, C.D. (1998). ESA1 is a histone acetyltransferase that is essential for growth in yeast. Proc. Natl. Acad. Sci. USA *95*, 3561–3565.

Struhl, K. (1998). Histone acetylation and transcriptional regulatory mechanisms. Genes Dev. *12*, 599–606.

Tercero, J.C., Riles, L.E., and Wickner, R.B. (1992). Localized mutagenesis and evidence for post-translational regulation of MAK3. J. Biol. Chem. *267*, 20270–20276.

Wade, P.A., Pruss, D., and Wolffe, A.P. (1997). Histone acetylation: chromatin in action. Trends Biochem. Sci. *22*, 128–132.

Wang, L., Liu, L., and Berger, S.L. (1998). Critical residues for histone acetylation by Gcn5, functioning in Ada and SAGA complexes, are also required for transcriptional function in vivo. Genes Dev. *12*, 640–653.

Williams, J.W., and Northrop, D.B. (1979). Synthesis of a tight-binding, multisubstrate analog inhibitor of gentamicin acetyltransferase I. J. Antiobiot. *32*, 1147–1154.

Wolodko, W.T., Fraser, M.E., James, M.N.G., and Bridgers, W.A. (1994). The crystal structure of succinyl-CoA synthetase from *Escherichia coli* at 2.5Å resolution. J. Biol. Chem. *269*, 10883–10890.

Yang, X.-J., Ogryzko, V.V., Nishikawa, J.-I., Howard, B.H., and Nakatani, Y. (1996). A p300/CBP-associated factor that competes with the adenoviral oncoprotein. Nature *382*, 319–324.

Brookhaven Protein Data Bank Accession Number

The coordinates for the structure described in this paper have been deposited with the accession number 1bo4. For immediate access to the atomic coordinates, contact S. K. B. (burley@rockvax.rockefeller.edu.).